DOI: 10.1002/adma.200702326

Nanoscale Patterning and Electronics on Flexible Substrate by Direct Nanoimprinting of Metallic Nanoparticles**

By *Inkyu Park*, *Seung H. Ko*, *Heng Pan*, *Costas P. Grigoropoulos*,* *Albert P. Pisano*,* *Jean M. J. Fréchet*, *Eung-Sug Lee*, and *Jun-Ho Jeong*

Recent years have witnessed an expanding interest in the application of flexible polymer materials (e.g., polyimide, polyester, etc.) as the substrates for electronic and display devices. These applications include flexible organic light-emitting displays,[1,2] thin film transistors,[3–5] sensors,[6,7] and polymer MEMS.[8,9] The advantages of polymer-based materials are their mechanical flexibility, light weight, enhanced durability, and low cost compared with rigid materials (such as silicon and quartz). However, it can be difficult to integrate polymers into an integrated circuit (IC) microfabrication process due to their low thermal stability (low melting and low glass transition temperatures) and solvent susceptibility. In practice, conventional IC fabrication processes are subject to limitations, in that they are multi-step, involve high processing temperatures, caustic baths and strong solvents.

In order to address the current problems of microfabrication on flexible substrate, many alternative approaches to conventional photolithography-based process have been introduced by a number of researchers. These include microcontact printing (μCP) combined with metal etching,[10] electroless plating,[11] electropolymerization,[12] and direct metal layer transfer[13] for the microscale metal patterning on flexible substrates. Stencil lithography[14] was mainly applied for dielectric layer patterning on polymer substrates for the formation of electrical capacitors[15,16] due to its limited resolution. Inkjet printing was used for a drop-on-demand patterning of conductive polymer PEDOT[17] and gold[18] layers for drain-source and gate electrodes. However, its best resolution is 20–50 μm[19,20] limited by the nozzle diameter, the statistical variation of the droplet flight, and spreading on the substrate.

Organic semiconducting materials are being widely used as semiconducting layers in flexible electronics due to their cost-effectiveness, mechanical flexibility, and ease of application via specific chemical modification. However, further channel size down-scaling is essential for better performance of organic field effect transistor due to the lower carrier mobility of the organic semiconducting materials. While the abovementioned methods cannot achieve ultrafine features (a few μm's down to ~ 100 nm) in high aerial density and good reproducibility, nanoimprinting lithography (NIL) allows easy fabrication of precise nanoscale structures. NIL has been applied for nanopatterning in various fields such as biological nanostructures,[21] nanophotonic devices,[22,23] organic electronics,[24,25] and the patterning of magnetic materials.[26] Especially, metal nanopatterning via nanoimprinting is widely employed in nanoscale electronics and biosensing platforms. However, metal nanoimprinting has been typically an indirect process where a polymer (e.g., PMMA) pattern is first created by nanoimprinting, and then used as a mask for metal film etching or metal lift-off process.[27] This involves multiple and expensive process steps and its chemistry is harsh for the flexible substrates. Furthermore, flexible substrates are not resistant to high temperature and pressure during the imprinting process. Recently, imprint resists based on monomer[28] or copolymer[29] have been developed and used for low pressure/low temperature nanoimprinting process. However, these are also indirect methods for metal nanopatterning. Very few direct metal nanoimprinting processes have been demonstrated so far due to the high melting temperature of metals. As an alternative to metal direct nanoimprinting, solid state embossing methods based upon plastic deformation of metal thin films have been introduced. These approaches involved either deformation of a metal film under very high pressure[30] or deformation of a metal thin film/polymer multilayer under relatively lower pressure.[31] Evidently, they are not compatible with flexible substrate since its mechanical strength is not sufficient for such processes. Additionally, these methods do not allow the fabrication of isolated, arbitrary features, and always leave unwanted residual layers.

To alleviate the limitations described in the fabrication processes above, the authors have recently developed a novel

[*] Prof. C. P. Grigoropoulos, Prof. A. P. Pisano, I. Park, Dr. S. H. Ko, H. Pan
Department of Mechanical Engineering
University of California, Berkeley, CA 94720 (USA)
E-mail: cgrigoro@me.berkeley.edu; appisano@me.berkeley.edu
Prof. J. M. J. Fréchet
College of Chemistry
University of California, Berkeley, CA 94720 (USA)
Dr. E.-S. Lee, Dr. J.-H. Jeong
Korea Institute of Machinery and Material (KIMM)
Daejon, 305-343 (Korea)

[**] I.P. and S.H.K. equally contributed to this work. The authors appreciate Prof. C. Luscombe (University of Washington) for providing semiconducting polymer material. Financial support to the University of California, Berkeley, by the Center for Nanoscale Mechatronics and Manufacturing(CNMM) (Grant No. 019997), one of the 21st Century Frontier Research Programs from the Ministry of Science and Technology, Republic of Korea, U.S. National Science Foundation (grant nos. CTS-0417563 and CMMI 0700827), and the U.S. Department of Energy (DE-AC03-76SF00098) is gratefully acknowledged.

ADVANCED MATERIALS

nanoparticle-based direct nanoimprinting process for metal nanopatterning on a rigid silicon substrate.[32] This process facilitates a very high throughput direct metal patterning in ultrafine nanoscale dimensions with very low pressure and temperature requirements, and process simplicity. Mixture of metal nanoparticles with organic solvents in a liquid form enables a flexible adjustment of fluid properties (eg. viscosity) during the nanoimprinting process. Very low viscosity of nanoparticle solution allows a high quality nanoimprinting performance with negligible residual layer under an extremely low imprinting pressure condition. Furthermore, this low pressure process is compatible with a flexible polymer-based nanoimprinting stamp, which is simple and inexpensive to replicate and very easy to handle. The thermodynamic size effect of metal nanoparticles facilitates much lower melting temperature of nanoparticles than those of bulk materials. Thus, thermal annealing at low temperatures can transform collections of discrete nanoparticles within nanoimprinted structures into conductive and continuous metal film. Owing to this low temperature and low pressure conditions, metal nanoparticle-based direct nanoimprinting process should be an excellent approach to the nanoscale patterning and electronics fabrication on flexible substrate for which low processing temperature and pressure are essential requirements. In this communication, we demonstrate a high-throughput and ultrafine patterning of metallic micro- and nanostructures for electronics on flexible substrates via a direct nanoimprinting process of metallic nanoparticles.

The direct nanoimprinting of metallic nanoparticles on flexible substrates is accomplished by the following steps (Fig. 1a): (i) the flexible substrate (e.g., polyimide) is cleaned, dehydrated, fixed on a rigid substrate and coated with poly(vinyl phenol) as a gate dielectric material; (ii) metal nanoparticle solution is dispensed on flexible substrate and imprinted by using polydimethylsiloxane (PDMS) stamp at low pressure (< 40 kPa) and low temperature (80 °C); (iii) After the solvent evaporation and cooling, PDMS stamp is demolded and imprinted metal nanoparticle patterns are heated up to 140 °C for 10 min to induce nanoparticle melting; (iv) finally the flexible substrate with nanoimprinted structures are released from the rigid substrate for usage. 2–3 nm sized gold nanoparticles (AuNPs) encapsulated by hexanethiol self-assembled monolayer (SAM) in organic solvent (α-terpineol) bear several critical functions in the current process. First, gold nanoparticles (AuNPs) in carrier solvent allow low temperature fabrication of metal component. The melting point of AuNPs is approximately 130–140 °C as verified by the evolution of electrical resistivity, reflectance, and mass of AuNP thin film.[32] This is much lower than that of bulk gold (1063 °C), and thus our method is compatible with the temperature restrictions of flexible substrates. Secondly, they allow low viscosity condition for nanoimprinting process without driving the processing temperature over bulk gold melting temperature (1063 °C). Moderate heating during the nanoimprinting process allows the nanoparticle solution to have a low viscosity and facilitates successful pattern replication with minimum residual layer. The imprinting processing temperature was optimized at 80 °C to achieve the best filling of the solution into the PDMS stamp. This was done by balancing the two events that alter the viscosity of the solution; firstly the decrease in viscosity that occurs with increasing temperatures, and secondly, the simultaneous increase in viscosity that takes place because of solvent evaporation at elevated temperatures. Flexible PDMS stamp is used instead of rigid stamp (e.g., silicon or quartz) because of its advantages as follows: (i) easy replication from original master structure, (ii) gas permeability for the evaporation of organic solvents during the nanoimprinting process, (iii) easy demolding process and less sensitivity to the contaminants on sample surface due to its flexibility. Figure 1b shows a camera image of gold micro/nanostructures and microelectronic circuits on polyimide substrate fabricated by metallic nanoparticle direct nanoimprinting. The current

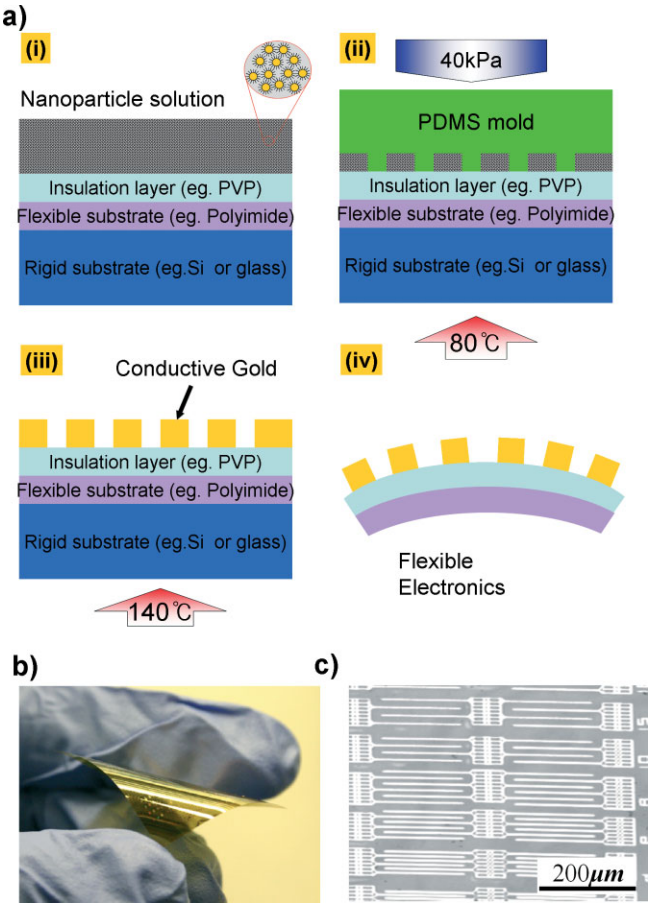

Figure 1. Overview of direct nanoimprinting process of gold nanoparticles: a) Procedure of direct nanoparticle nanoimprinting: (i) fix a clean flexible substrate onto a rigid substrate and dispense nanoparticle solution (inset picture is the magnified schematics of SAM protected AuNPs) (ii) nanoimprinting with PDMS stamp (iii) nanoparticle melting process (iv) release of flexible substrate; b) Photo of electrical devices nanoimprinted on polyimide substrate. c) Optical micrograph of microscale electrical structures (source-drain electrodes for multichannel transistors) on a polyimide substrate fabricated by direct nanoimprinting of gold nanoparticle solution.

process facilitated parallel and high-throughput (total processing time < 30 min) manufacturing of ultrafine structures with minimal residual layer and good uniformity on flexible substrate with an area of up to 2 × 2 cm^2. The imprinted structures maintained good adhesion to the polyimide substrate and geometrical shapes after multiple cycles of bending and tensile deformation. Figure 1c shows an optical micrograph of patterned gold microstructures on polyimide substrate. These particular structures shown here are source-drain electrodes for multichannel transistor devices.

In order to prove the feasibility and utility of the direct metal nanoparticle nanoimprinting process at the microscale, a variety of microscale gold structures were fabricated as shown in Figure 2. Sub-micrometer wires are shown in Figure 2a with triangular cross-sectional geometry (full width at half maximum (FWHM) = 750 nm, maximum height = 405 nm, and separation pitch = 4 μm). Compared to the corresponding patterns (FWHM = 750 nm, height = 1 μm, pitch = 4 μm) in the PDMS stamp, the nanoimprinted patterns show faithful replication of stamp features except for the height shrinkage. This shrinkage in vertical direction may be due to either the reflow and densification of the nanoparticle solution during the melting process, incomplete filling of gold nanoparticle solution into the PDMS stamp, or deformation of the PDMS stamp by the applied pressure. Also, the mass of gold nanoparticles is only ~ 10 % of the entire gold nanoparticle imprinting solution while the majority of the mass is from the α-terpineol solvent. Therefore, the solvent evaporation will leave gold nanoparticles behind with volume shrunk from original volume of the nanoimprinting solution within the imprinting stamp. Figure 2b shows an array of gold microwires (FWHM = 2.5 μm, height = 350 nm, pitch = 8 μm). The cross-section of the nanoimprinted microwire is similar to trapezoidal shape but its edge locations are slightly raised (height = 420 nm) and the center portion is flat and lowered (height = 350 nm). This cross-sectional geometry ("rabbit ear"-like shape) may be due to incomplete filling of nanoparticle solutions and wetting on the PDMS stamp surface. The edge portions are dominated by the capillary force at the interface between the nanoimprinting solution and the stamp, while the center portion is dominated by the gravitational force applied on the solution. Other microscale structures such as array of circular microholes (Fig. 2c, diameter = 4.5 μm, pitch = 8.0 μm) and rectangular microdots (Fig. 2d, width = 2 μm, pitch = 8.0 μm) were also successfully fabricated. The absence of the residual layer is very critical for direct nanoimprinting without using any post processing especially in the area of the high performance electronics application. Characterization via AFM and SEM-EDX as well as electrical measurements were performed to verify the absence of the residual layer. AFM figures in Figure 2a–d show no visible traces of gold residuals. The SEM-EDX mapping (Fig. 2e and f)) of gold (Au) elements shows that the Au_M line in EDX spectra exists only at the imprinted features while no or negligible signal is found in the remaining regions. The gold (Au) element mapping exactly follows the shape of imprinted features with no significant residual layers. Here, bright dots (bottom row pictures) on the imprinted features indicate the existence of Au_M line in EDX spectra while dark color on the surrounding regions means no or negligible gold residual layers.

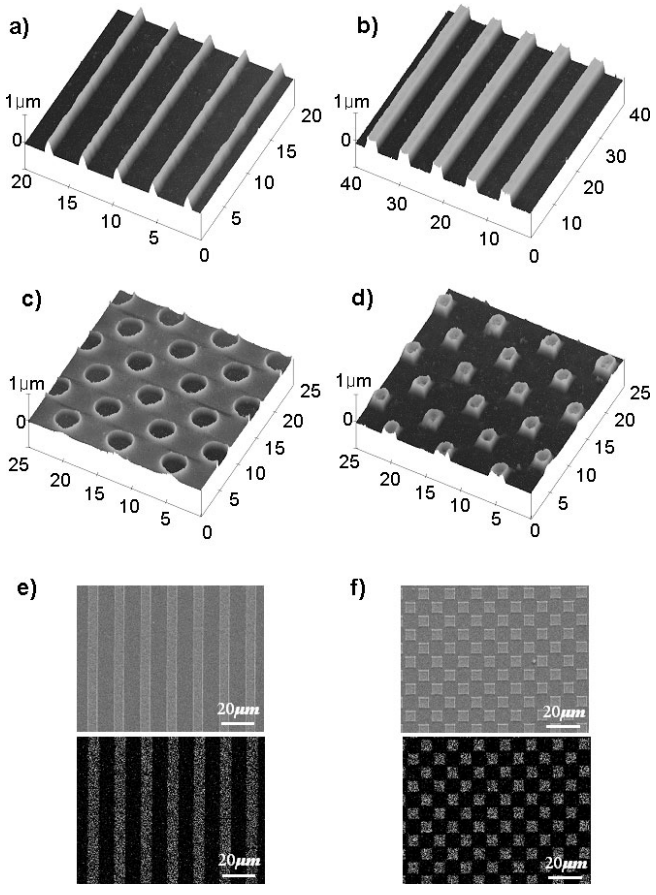

Figure 2. Microscale gold structures on polyimide substrate fabricated by direct nanoimprinting of gold nanoparticles: a), b) Array of microwires (a: width = 750 nm, pitch = 4 μm; b: width = 2.5 μm, pitch = 8 μm); c) Array of microholes (diameter = 4.5 μm, pitch = 8 μm); d) Array of microdots (width = 2 μm, pitch = 8 μm); e), f) SEM-EDX analysis of nanoimprinted structures by gold (AuM line) element mapping. Bright dots in bottom row pictures indicates the existence of AuM line in EDX spectra while dark color verifies no or negligible gold residual layers in the surrounding regions.

The electrical measurement between neighboring microstructures also verified that they are electrically isolated from each other. Therefore, it can be concluded that our direct nanoimprinting process does not require any additional steps for the removal of residual layers after the imprinting process. The minimal residual layer can be attributed to two factors in the nanoimprinting process: (1) optimization of the nanoparticle solution fluidic properties (low viscosity and surface tension at the imprinting temperature around 80 °C), (2) good surface contact between the PDMS imprinting stamp and the flexible polyimide substrate due to the flexibility of the stamp.

To explore the limits of the minimum feature size achievable in the direct nanoimprinting process, ultrafine structures

ADVANCED MATERIALS

in nanoscale dimensions were fabricated on flexible substrate. Figure 3a shows an array of gold nanowires (FWHM = 75 nm, pitch = 150 nm, height = 25.7 nm). Although there is some nonuniformity in the height (min = 16.1 nm, average = 25.7 nm, max = 30.7 nm) along the length direction of the gold nanowires, this result shows that a very dense array of nanoscale patterns can be replicated very easily and faithfully by direct nanoimprinting. Figure 3b shows that a dense array of gold nanodots (FWHM = 80 nm, pitch = 200 nm, height = 32.4 nm) was successfully fabricated with no visible defects. The heights of the nanodots are found to be reasonably uniform (average = 32.4 nm, standard deviation = 2.8 nm). This kind of structure has a great potential for applications in the surface enhanced Raman spectroscopy (SERS) on flexible substrates since the size and gap of the metal nanodots can be easily controlled with high uniformity by modifying the design of the nanoimprinting stamps. The average height (32.4 nm) of nanodots is slightly larger than that (25.7 nm) of the nanowire array. This may be because the filling of nanoparticle solution was more effective, being assisted by the capillary force from four side walls of the nanodot features in the nanoimprinting stamp while the capillary force from only two side walls existed in the nanowire array features. The advantage of direct nanoimprinting is that it can generate micro/nano-structures in a variety of dimensions and arbitrary design. Figure 3c and d provide good examples of nanostructures in arbitrary designs. The "*Cal*" mark and the word "NANO" were successfully patterned in an area of 2.7 μm × 2.2 μm and 3.0 μm × 0.8 μm respectively with smallest line width of 80 nm at the location (3). These two images show that the direct nanoimprinting of metal nanoparticle solution faithfully transfers patterns of nanostructures with arbitrary design and various nanoscale dimensions with good fidelity.

For the practical application of the nanoimprinted metal structures in flexible electronics, their electrical characteristics are the most important factor. First, current-voltage (*I–V*) curve (Fig. 4a) along a single gold microwire (width = 2 μm, length = 200 μm, height = 300 nm) shows that the imprinted structure behaves as a good ohmic resistor with linear *I–V* relation (R = 66.4 Ω). In addition, electrical isolation was measured to check any possible leakage current via residual layer between resistors (3.5 μm width, 3.5 μm gap between wires). However, no measurable current was found (< 1 nA, equivalent to the noise level). This proves that two neighboring wires fabricated by direct nanoimprinting process are very well isolated electrically. The electrical resistivity of the nanoimprinted and thermally annealed gold microstructures (total 53 gold microwires in 4–8 μm width and 200 μm length) has an average of $\langle\rho\rangle = 1.99 \times 10^{-7}$ Ω·m with a standard deviation of $\sigma_\rho = 5.73 \times 10^{-8}$ Ω·m. This average resistivity is about 8 times higher than that of bulk gold (2.4×10^{-8} Ω·m). This could be due to incomplete evaporation of solvent and the desorption of the hexanethiol layer between nanoparticles acting as a dielectric layer. Especially, the carbon (C) and sulfur (S) element peaks from SEM-EDX image and XPS analysis show that significant amount of carbon and sulfur from hexanethiol remain in the film even after thermal annealing process. Enhanced carrier scattering in the presence of a polycrystalline structure and rough surface (R_{rms} ~ 5 nm) may also contribute to the high resistivity. However, this is still a resistivity low enough for the usage as electrical component in high performance/speed electronics. The histogram of resistivity (Fig. 4b) shows a broad distribution ($\rho_{min} = 1.07 \times 10^{-7}$ Ω·m and $\rho_{max} = 3.12 \times 10^{-7}$ Ω·m) around the average value, which could be explained by different degree of nanoparticle melting and desorption of hexanethiol layer at different locations, as well as by the varying contact conditions during the electrical probing.

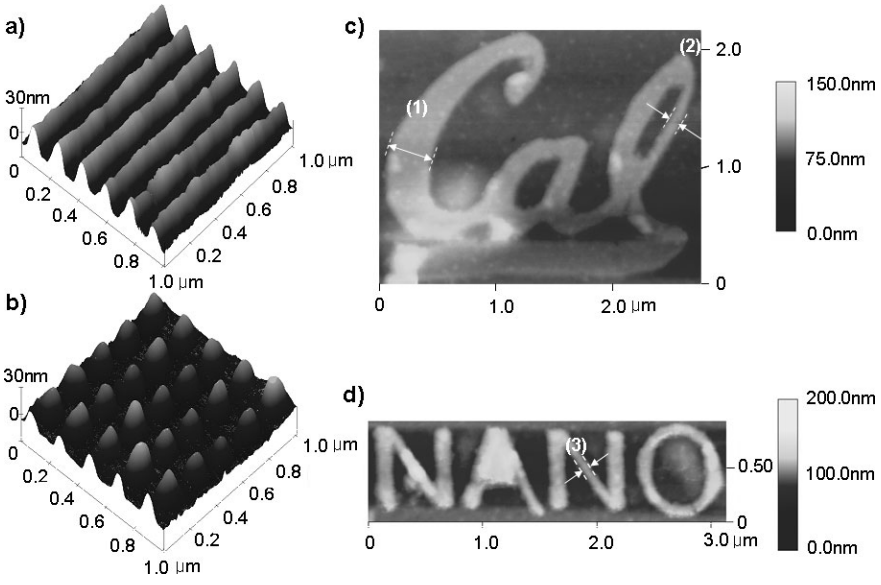

Figure 3. Nanoscale gold structures on polyimide substrate fabricated by direct nanoimprinting of gold nanoparticles a) Array of gold nanowires (width = 75 nm, pitch = 150 nm. b) Array of gold nanodots (width = 80 nm, pitch = 200 nm). c) "Cal" pattern in nanoscale dimension. Width (1) = 400 nm, (2) = 100 nm. d) "NANO" pattern in nanoscale dimension. Width at (3) = 80 nm.

Second, organic field effect transistors (OFETs) were fabricated and characterized. Two types of transistor configurations (single channel transistors and multiple channel transistors) were fabricated by direct nanoimprinting. Figure 4c–i shows the schematics of a single channel transistor with nanoimprinted source/drain electrodes, spincoated air stable semiconducting polymer, spincoated PVP dielectric layer, and evaporated Al gate on polyimide substrate. OFETs with various channel lengths (2/4/6/8/10/12/16/20/30/50 μm) and 160 μm channel width were

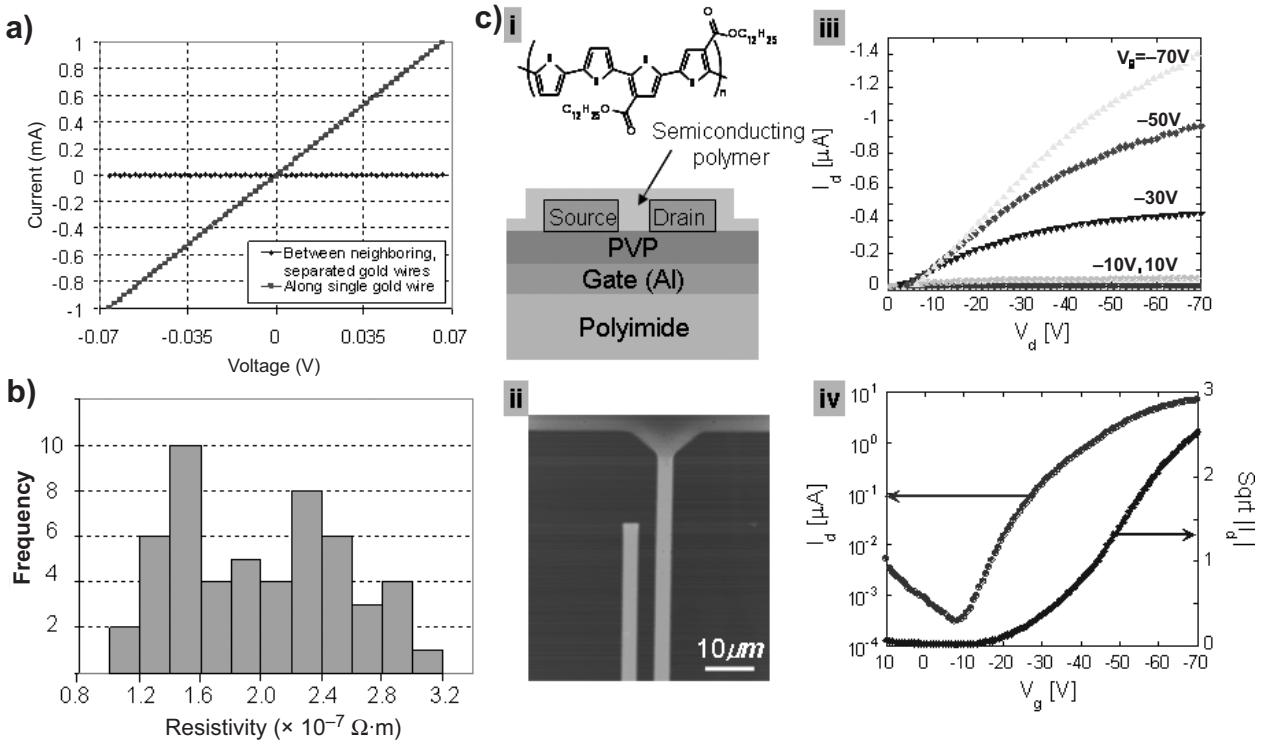

Figure 4. Electrical characterization of directly nanoimprinted Au structures. a) *I–V* curves along single Au microwire (width = 2 μm, square symbol) and between two neighboring Au microwires (width = 3.5 μm, gap = 3.5 μm, circular symbol); b) Histogram of electrical resistivity of nanoimprinted Au structures; c) Organic field effect transistor (OFET). i) Schematics of organic field effect transistor. Source/drain electrodes are fabricated by direct nanoimprinting of Au nanoparticles; gate voltage is applied by Al back-gate electrode underneath poly-vinyl-propyl (PVP); semiconductor channel is made via spin coating of air-stable organic semiconductor thin film. ii) AFM image of OFET. iii) Output and iv) transfer characteristics of a nanoimprinted OFET ($L \sim 4$ μm, $W \sim 160$ μm). For output characteristics measurement, the drain voltage (*Vd*) was scanned from 0 to –70 V and the drain current (*Id*) was measured while gate voltage (*Vg*) was fixed at –70, –50, –30, –10, 10 V during each *Vd* scanning. For transfer characteristics measurement, the gate voltage (*Vg*) was scanned from 10 to –70V and the drain current (*Id*) was measured while drain voltage (*Vd*) was fixed at –70 V.

fabricated. Figure 4c-ii shows an AFM topography image of a 4 μm single channel. The OFET output and transfer characteristics are shown in Figure 4c-iii, iv for 4 μm channel length. The OFET shows typical output and transfer characteristics with operation in p-type accumulation mode with I_{on}/I_{off} ratio of 10^3–10^4 and threshold voltage (V_t) of –25 V. The mobility extracted from the saturated transfer characteristics[33] of the OFET was found to be around 0.001–0.002 $cm^2 \cdot V^{-1}\ s^{-1}$ which is slightly lower than the nanoimprinted OFET sample on SiO_2/p+ Si wafer (0.004–0.006 $cm^2 \cdot V^{-1}\ s^{-1}$).[32] The nanoparticle nano-imprinting can produce very short channels (micrometer to submicrometer) with high drain current. However, this very short channel showed short channel effect without current saturation.

Due to the flexibility of the polymer substrate, the devices are easily subject to a variety of mechanical deformation conditions (e.g., bending, compression, and tension). These may degrade the structural and electrical characteristics of flexible electronics. For this reason, electrical and structural characterization of nanoimprinted gold structures on flexible substrate was performed under a cyclic bending deformation, which is the most common condition for the flexible electronics. Figure 5a shows the experimental setup for the cyclic bending deformation of flexible electronics with nanoimprinted gold structures. By fixing one end (right) and moving another end (left) in a cyclic motion and modifying sample carrier properly to simulate simple supported (hinged) end configuration, a uniform bending deformation (same radius of curvature) throughout the entire flexible substrate could be created. As shown in Figure 5a-ii,iii, bending deformation cycles with radius of curvature between $\kappa_{min} = 7.48$ mm (large deflection) and $\kappa_{max} > 400$ mm (small deflection) were run from zero to 65000 cycles. The cyclic motion of the actuator was a triangular wave with a frequency of $f = 0.7$ Hz. SEM images in Figure 5b compare nanoimprinted gold microstructures (i-line array, ii-hole array) before and after 65000 cycles of bending deformation. The microstructures maintained the same surface morphology with no observable development of micro/nanoscale cracks or change of surface roughness after 1k, 15k, and 65k cycles of bending deformation. The electrical resistivities of the nanoimprinted gold microwires in 4–8 μm width and 200 μm length were measured for different bending cycles (0, 1k, 15k, 65k cycles). As shown in Figure 5c, the resistivity values do not show any changes through the course of bending deformation cycles. Although the average of resistivity changes slightly ($\rho = 1.99 \times 10^{-7}$ Ω·m for 0 cycle,

ADVANCED MATERIALS

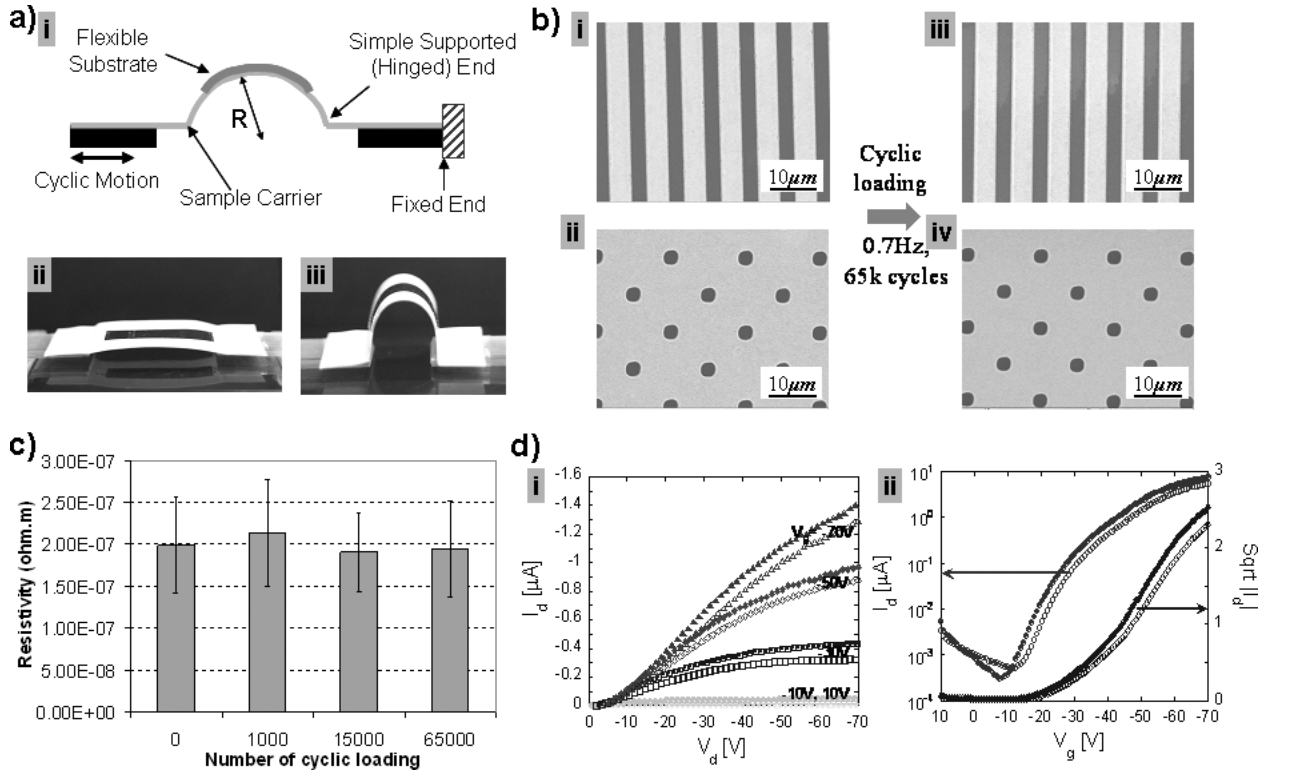

Figure 5. Electrical and structural characterization of nanoimprinted Au structures on flexible substrate under cyclic bending deformation. a) Test setup of cyclic loading and picture of minimum and maximum bending deformation of sample carrier of flexible substrate; b) No visible changes of surface morphology are observed after cyclic bending test for 65k cycles; c) No changes in average resistivities are observed after 1k-65k bending cycles. d) No significant change of output (i) and transfer (ii) characteristics of OFET after 20k cycles is observed (before: filled symbols, after: empty symbols). The scanning condition is same with Figure 4c.

$\rho = 2.13 \times 10^{-7}$ Ω·m for 1k cycles, $\rho = 1.90 \times 10^{-7}$ Ω·m for 15k cycles, and $\rho = 1.94 \times 10^{-7}$ Ω·m for 65k cycles), the changes of the average are much smaller than the standard deviation. Therefore, we can conclude that there is no observable statistical change of the electrical resistivity by the long period bending deformation cycles.

Besides SEM observation and electrical resistivity measurement, the transistor performance characteristics were measured before and after the 20k bending cycles. Figure 5d shows (i) output characteristics and (ii) transfer characteristics of OFETs on polyimide substrate before cyclic loading (filled symbols) and after 20k bending cycles (empty symbols) for a 4 μm single channel. No significant changes in the OFET performance were observed except slight drop in drain current probably due to the semiconductor polymer degradation during the high voltage measurement. Similar OFET performance signifies that the electrical performance of the devices fabricated by the current process is reasonably good for application to flexible electronics.

In summary, we successfully fabricated micro/nanoscale metallic structures on flexible polymer substrate by direct nanoimprinting of metallic nanoparticle solution for high resolution flexible electronics fabrication. Easy control of the fluidic viscosity of α-terpineol-based gold nanoparticle solution and the low melting temperature of gold nanoparticles facilitates low temperature and low pressure process, which is perfectly compatible with flexible polymer electronics. Various microstructures of gold such as microwires, microholes, and microdots were fabricated with no or negligible residual layer between the nanoimprinted features. This minimal residual layer is believed to be due to low viscosity and surface wetting of gold nanoparticle solution as well as the conformal surface contact between the PDMS stamp and the flexible substrate. Nanoscale structures such as gold nanowires, nanodots, and arbitrary designs with minimum feature size of 75 nm have also been successfully fabricated. Organic field effect transistors (OFETs) were demonstrated by using air-stable semiconducting polymer and nanoimprinted gold source-drain electrodes on flexible polymer substrate with good output and transfer characteristics. Lastly, the influence of mechanical bending on nanoimprinted electrical structures (resistors and transistors) was characterized. By cyclic bending deformation test, it was found that the nanoimprinted gold structures were mechanically robust with no observable micro/nanoscale crack development and electrical resistivity increase. Also, OFET devices on flexible substrate showed no significant changes in their performances after the cyclic loading. It is expected that the current approach based on direct nanoim-

printing of metallic nanoparticles can provide a very simple and effective nanoscale patterning tool for a variety of functional nanoparticles and enable extremely low-cost, high-throughput, ultrafine resolution manufacturing on flexible polymer substrates.

Experimental

Gold Nanoparticle Synthesis and Solution Preparation: The gold nanoparticles were prepared by a two-phase reduction method [34]. Aqueous metal salts ($HAuCl_4$) were mixed in a toluene solution containing long-chain alkylammonium surfactants to form a two-phase system. 1.5 g of tetroactylammonium bromide ($C_{32}H_{68}BrN$) was mixed with 80 mL of toluene and added to 0.31 g of hydrogen tetrachloroaurate (III) hydrate ($HAuCl_4 \cdot H_2O$) in 25 mL of deionized (DI) water. Vigorous stirring transferred the metal salt ($AuCl_4^-$) into the organic phase (toluene) and the aqueous phase was removed. A measured quantity of capping agent, a long-chain thiol (hexanethiol), was added to the gold solution while stirring. Then, a reducing agent, sodium borohydride ($NaBH_4$), mixed in 25 mL of water was added into the organic phase with a fast addition over approximately 10 s to nucleate nano-crystals. The mixture reacted at room temperature for three and a half hours. The toluene was removed with a rotary evaporator and the leftover black particles suspended in ethanol and sonicated briefly. The particles were washed with ethanol and acetone and air dried. The average nano-crystal size is 1–3 nm and the size is coarsely tunable by adjusting the ratio of capping groups to metal salt, whereas size selective precipitation is employed to narrow the initial size distribution. In this method, the size distribution of synthesized nanoparticles is controlled by the ratio between metal salt and surface monolayer that additionally prevents the agglomeration of nanoparticles. The size of synthesized nanoparticles is distributed from 1 to 3 nm as measured by TEM. Monolayer-protected gold nanoparticles are suspended in α-terpineol with 10 % in weight.

PDMS Stamp Fabrication: The fabrication of PDMS stamp with microscale patterns was performed by the following procedure: (1) The silicon wafer was cleaned with piranha solution and with an O_2 plasma, and treated with SAM hexamethyldisilazane (HMDS) to enhance the adhesion of photoresist on the substrate. (2) 1.3 μm thick G-line positive photoresist (OCG825, Arch Chemicals, Inc., Columbus, OH) was spin coated onto the silicon wafer. (3) 4 x reduction lithography (FPA-141F, Canon Inc., Japan) was used for the patterning of microscale features followed by developing with G-line developer (OCG 934, Arch Chemicals, Inc.). (4) After hardbaking at 120 °C, the silicon master was coated with 10 nm thick polytetrafluoroethylene (PTFE) using a vapor phase deposition system (Advanced Silicon Etch System, Surface Technology Systems, UK) to prevent the stiction of PDMS to the silicon master. (5) 10:1 (PDMS:curing agent) mixture of Sylgard 184 silicone elastomer kit (Dow Corning, Midland, MI) was poured on the silicon master. (6) It was degassed at room temperature and atmospheric pressure for 1 h and cured at 70 °C for 2 h. (7) After curing, the PDMS stamp was carefully released from silicon master. In the fabrication of stamp with nanoscale features, steps (1)–(3) were replaced with electron-beam lithography on 200 nm thick Poly(-methyl methacrylate) (PMMA), electron beam deposition and lift-off of 15 nm thick Cr layer, and reactive ion etching (CHF_3+Ar) of SiO_2 film by 50 nm depth.

Semiconducting Polymer Synthesis: All chemicals were purchased from Aldrich and used without further purification unless otherwise noted. All solvents were purified on a solvent purification system. All reactions were performed under N_2 unless otherwise noted. All extracts were dried over anhydrous $MgSO_4$ and solvents were removed by rotary evaporation with vacuum assist. Flash chromatography was performed using Merck Kieselgel60 (230–400 mesh) silica. ^1H NMR spectra were recorded with Brüker AMX-300, AM-400 or DRX-500 instruments using $CDCl_3$ as the solvent unless otherwise noted. Analytical size exclusion chromatography (SEC) in THF was performed at 35 °C at a nominal flow rate of a 1.0 mL·min^{-1} on a chromatography line calibrated with linear polystyrene standards (162–2100000 Da) and fitted with three 7.5 × 300 mm PL gel columns (5 μm particle size). The columns have a pore size of 105, 103, and 500 Å, respectively. The SEC system consists of a Waters 510 pump, a Waters 717 autosampler, and a Waters 486 UV-Vis detector detecting at 254 and 450 nm. Polymer solutions were prepared by adding 100 μL of a 1 mg·mL^{-1} solution of the polymer in *o*-DCB to 1 mL of THF, then filtering through 0.2 μm pore size PVDF filters (Whatman) before injection.

Electrical Measurement: The current-voltage relation, electrical resistivity of nanoimprinted gold wires, and output and transfer characteristics of OFET device were measured using HP4155A semiconductor parameter analyzer and a probe station with the micro-positioning manipulators and tungsten probe tip (10 μm tip diameter) in a dark Faraday cage in air.

Received: September 13, 2007
Revised: November 11, 2007
Published online: January 17, 2008

[1] J.-W. Kang, W.-I. Jeong, J.-J. Kim, H.-K. Kim, D.-G. Kim, G.-H. Lee, *Electrochem. Solid-State Lett.* **2007**, *10*, 75.
[2] L. Hou, Q. Hou, Y. Mo, J. Peng, Y. Cao, *Appl. Phys. Lett.* **2005**, *87*, 243504.
[3] S. H. Ko, H. Pan, C. P. Grigoropoulos, C. K. Luscombe, J. M. J. Fréchet, D. Poulikakos, *Nanotechnology* **2007**, *18*, 345202.
[4] U. Haas, H. Gold, A. Haase, G. Jakopic, B. Stadlober, *Appl. Phys. Lett.* **2007**, *91*, 043511.
[5] A. L. Briseno, S. C. B. Mannsfeld, M. M. Ling, S. Liu, R. J. Tseng, C. Reese, M. E. Roberts, Y. Yang, F. Wudl, Z. Bao, *Nature* **2006**, *444*, 913.
[6] V. Shamanna, S. Das, Z. Celik-Butler, K. L. Lawrence, *J. Micromech. Microeng.* **2006**, *16*, 1984.
[7] F. Jiang, G.-B. Lee, Y.-C. Tai, C.-M. Ho, *Sens. Actuators A* **2000**, *79*, 194.
[8] S. A. Dayeh, D. P. Butler, Z. Celik-Butler, *Sens. Actuators A* **2004**, *118*, 49.
[9] S. Tung, S. R. Witherspoon, L. A. Roe, A. Silano, D. P. Maynard, N. Ferraro, *Smart Mater. Struct.* **2001**, *10*, 1230.
[10] J. A. Rogers, Z. Bao, K. Baldwin, A. Dodabalapur, B. Crone, V. R. Raju, V. Kuck, H. Katz, K. Amundson, J. Ewing, P. Drzaic, *Proc. Natl. Acad. Sci. USA* **2001**, *98*, 4835.
[11] U. Zschieschang, H. Klauk, M. Halik, G. Schmid, C. Dehm, *Adv. Mater.* **2003**, *15*, 1147.
[12] M. Schoenfisch, J. E. Pemberton, *Langmuir* **1999**, *15*, 509.
[13] Z. Wang, J. Yuan, J. Zhang, R. Xing, D. Yan, Y. Han, *Adv. Mater.* **2003**, 15, 1009.
[14] N. Takano, L. M. Doeswijk, M. A. Boogaart, J. Auerswald, H. F. Knapp, O. Dubochet, T. Hessler, J. Brugger, *J. Micromech. Microeng.* **2006**, *16*, 1606.
[15] K. Arshak, D. Morris, A. Arshak, O. Korostynska, E. Jafer, *Mater. Sci. Eng. C* **2006**, *26*, 1077.
[16] S. Cho, K. Jang, J. Hyun, S. Lee, K. Paik, H. Kim, J. Kim, *IEEE Trans. Electron. Packag. Manuf.* **2005**, *28*, 297.
[17] M. F. Mabrook, C. Pearson, M. C. Petty, *IEEE. Sens. J.* **2006**, *6*, 1435.
[18] S. Ko, J. Chung, H. Pan, C. P. Grigoropoulos, D. Poulikakos, *Sens. Actuators A* **2007**, *134*, 161.
[19] H. Sirringhaus, T. Kawase, R. H. Friend, T. Shimoda, M. Inbasekaran, W. Wu, E. P. Woo, *Science* **2000**, *290*, 2123.
[20] S. H. Ko, H. Pan, C. P. Grigoropoulos, C. K. Luscombe, J. M. J. Fréchet, D. Poulikakos, *Appl. Phys. Lett.* **2007**, *90*, 141103.

[21] I. Park, J. Cheng, E.-S. Lee, J.-H. Jeong, A. P. Pisano, *Appl. Phys. Lett.* **2007**, *90*, 093902.
[22] K. Nakamatsu, S. Matsui, *Jpn. J. Appl. Phys. Part 2* **2006**, *45*, L546.
[23] J. Seekamp, S. Zankovych, A. H. Helfer, P. Maury, C. M. Sotomayor Torres, G. Boettger, C. Liguda, M. Eich, B. Heidari, L. Montelius, J. Ahopelto, *Nanotechnology* **2002**, *13*, 581.
[24] W. Wu, G.-Y. Jung, D. Olynick, J. Straznicky, Z. Li, X. Li, D. Ohlberg, Y. Chen, S.-Y. Wang, J. Liddle, W. Tong, R. S. Williams, *Appl. Phys. A* **2005**, *80*, 1173.
[25] C. Kim, M. Stein, S. R. Forrest, *Appl. Phys. Lett.* **2002**, *80*, 4051.
[26] W. Wu, B. Cui, X. Y. Sun, W. Zhang, L. Zhuang, S. Y. Chou, *J. Vac. Sci. Technol. B* **1998**, *16*, 3825.
[27] C. M. Sotomayor Torres, *Alternative Lithography*, Springer, New York **2003**.
[28] H. Lee, S. Hong, K. Yang, K. Choi, *Microelectron. Eng.* **2006**, *83*, 323.
[29] S.-C. Hsu, W.-C. Liao, J.-C. Lin, *Microelectron. Eng.* **2007**, *84*, 129.
[30] H. Yoshihiko, U. Toshihiko, K. Tomohiro, M. Takashi, *Proc. SPIE-Int. Soc. Opt. Eng.* **2003**, *5220*, 74.
[31] H. L. Chen, S. Y. Chuang, H. C. Cheng, C. H. Lin, T. C. Chu, *Microelectron. Eng.* **2006**, *83*, 893.
[32] S. H. Ko, I. Park, H. Pan, C. Grigoropoulos, A. P. Pisano, C. K. Luscombe, J. M. J. Fréchet, *Nano Lett.* **2007**, *7*, 1869.
[33] R. F. Pierret, *Semiconductor Device Fundamentals*, Addison Wesley, New York **1996**.
[34] M. J. Hostetler, J. E. Wingate, C. J. Zhong, H. E. Harris, R. W. Vachet, M. R. Clark, J. D. Nondono, S. J. Green, J. J. Stokes, G. D. Wignall, G. L. Glish, M. D. Porter, N. D. Evans, R. W. Murray, *Langmuir* **1998**, *14*, 17.

